Bioorganic & Medicinal Chemistry xxx (2016) xxx–xxx

Contents lists available at ScienceDirect

Bioorganic & Medicinal Chemistry

journal homepage: www.elsevier.com/locate/bmc

Synthesis and evaluation of styrylpyran fluorophores for noninvasive detection of cerebral β-amyloid deposits

Bi-yue Zhu [a], Yan Cheng [a,*], Guo-bo Li [b], Sheng-yong Yang [b], Zhi-rong Zhang [a]

[a] Key Laboratory of Drug Targeting and Drug Delivery Systems, West China School of Pharmacy, Sichuan University, Chengdu 610041, China
[b] State Key Laboratory of Biotherapy/Collaborative Innovation Center of Biotherapy, West China Hospital, West China Medical School, Sichuan University, Chengdu 610041, China

ARTICLE INFO

Article history:
Received 16 October 2015
Revised 3 December 2015
Accepted 5 January 2016
Available online xxxx

Keywords:
β-Amyloid deposits
Optical imaging
Fluorophore
Styrylpyran

ABSTRACT

The development of amyloid-specific fluorophores allows the visualization of cerebral β-amyloid deposits using optical imaging technology. In the present study, a series of smart styrylpyran fluorophores with compact donor–acceptor architecture were designed and evaluated for noninvasive detection of cerebral β-amyloid deposits. Spectral behavior of the fluorophores changed significantly (optical turn-on) upon binding to β-amyloid aggregates. Computational studies were conducted to correlate the experimental K_d values with calculated binding energies, speculating the relationship between fluorophore structure and β-amyloid affinity. In vivo studies demonstrated that **PAD-2** could discriminate APP/PS1 transgenic mice from wild type controls, with specific labeling of cerebral β-amyloid deposits confirmed by ex vivo observation. Collectively, these styrylpyran fluorophores could provide a new scaffold for the development of optical imaging probes targeting cerebral β-amyloid deposits.

1. Introduction

Alzheimer's disease (AD) is the most common progressive neurodegenerative disease that poses an increasingly prevalent global health care challenge. The lack of effective therapeutics has been attributed to unspecified etiology of AD and late-stage administration. Cerebral β-amyloid deposits, composed of extracellular aggregated β-amyloid peptides, have been widely viewed as an important pathological hallmark of AD.[1–3] As β-amyloid deposition in the brain occurs prior to the earliest clinical symptoms, monitoring cerebral β-amyloid deposits in vivo would facilitate the elucidation of AD pathogenesis, prediction of AD progression, and evaluation of the efficacy of anti-amyloid therapeutics.

Neuroimaging techniques present immense potential for visualizing β-amyloid deposits in living brains.[4,5] Over the past few years, positron emission tomography (PET) imaging of cerebral β-amyloid deposits using amyloid-specific probes has been most widely studied.[6–16] Despite its tremendous success in human studies, the use of PET imaging in preclinical animal models for AD remains constrained by considerations of limited availabilities of radioisotopes and complexity of experimental procedures in radiolabeling and data acquisition. In contrast, simple and convenient optical imaging technique, which has been one of the most important tools in biological research, would be an attractive alternative to PET imaging of β-amyloid deposits in animal models.

To visualize cerebral β-amyloid deposits by in vivo optical imaging, fluorescence probes are required to obtain high target-to-background ratio.[17,18] Congo red (CR) and thioflavin T (ThT) are two well-known fluorescent dyes for β-amyloid deposits, providing most standardized way of post mortem histological analysis of AD brains; however, the bulky and charged molecules are not capable of penetrating blood brain barrier, which is critical for in vivo cerebral imaging. To detect cerebral β-amyloid deposits in vivo, design criteria of fluorescence probes are more stringent, including: rapid uptake in the brain (small molecular size with suitable lipophilicity), specific labeling of β-amyloid deposits (high-affinity binding), as well as substantial changes in fluorescence properties of bound forms of the probe (large Stokes shift, and change in fluorescence intensity). In the past few years, several advances have been made in the development of noninvasive fluorescence probes, such as AOI987,[19] NIAD-4,[17] THK-265,[20] DANIR-2c,[21] CRANAD series (CRANAD-2, CRANAD-58),[22,23] ANCA series,[24,25] and BODIPY series (BODIPY-7, BAP-1, BAP-2).[26–28] Although most of the probes are proven to show selective labeling of β-amyloid deposits in vivo, the intrinsic properties (short emission wavelength, moderate amyloid affinity, low washout from the brain, no bathochromic shift) may limit the potential use of these reported probes. More recently, fluorescence probes with push–pull architecture, such as BBTOM-3, DANIR-3b, and DTM-2 have been developed with improved emission wavelengths and proven

* Corresponding author. Tel.: +86 28 85501566; fax: +86 28 85501615.
E-mail address: yancheng@scu.edu.cn (Y. Cheng).

http://dx.doi.org/10.1016/j.bmc.2016.01.004
0968-0896/

to be efficient for the discrimination between transgenic and wild-type mice in vivo.[29–31] Although BBTOM-3 and DTM-2 were reported as promising fluorescence probes for cerebral β-amyloid deposits, the low fluorescence quantum yields may limit spatial resolution for in vivo imaging. Moreover, DTM-2 exhibited moderate affinity for β-amyloid aggregates. DANIR-3b displayed high sensitivity in detecting β-amyloid deposits and could differentiate transgenic mice from wild-type controls at an early time postinjection, which is beneficial for high-throughout screening of anti-amyloid therapies.

Recently, we have reported styrylpyran derivative **PAD-1** as a potential fluorescence probe targeting cerebral β-amyloid deposits. The fluorophore contains a conjugated π system with electron-donor (D) and electron-acceptor (A) groups as terminal moieties (Fig. 1).[32] The fluorophore displayed good binding affinity for β-amyloid fibrils, indicating that styrylpyran may serve as a new scaffold for the development of fluorescence probes for visualizing β-amyloid deposits in vivo. In the present study, a series of styrylpyran derivatives were designed and evaluated to study the binding affinity for cerebral β-amyloid deposits and kinetics in the brain. Herein we report the biological evaluation and structure–activity relationship of these styrylpyran derivatives as potential fluorescence probes for noninvasive detection of cerebral β-amyloid deposits.

2. Results and discussion

2.1. Chemistry

Molecular design of styrylpyran derivatives was aimed to obtain compact amyloid-specific fluorophores with suitable emission wavelengths. Dimethylamino and cyano group have been widely used as optimal D and A group, respectively, and were selected for the molecular design. Donor–acceptor (D–A) and donor–acceptor–donor (D–A–D) architecture with extended π conjugated bridges were designed to reduce the HOMO–LUMO gap for desired long emission wavelength to avoid autofluorescence. The key step in the formation of styrylpyran backbone was achieved by the condensation of pyran or benzopyran with appropriate aromatic aldehydes (Scheme 1).[33]

2.2. Spectroscopic profile

Long emission wavelengths and high fluorescence quantum yields are crucial for in vivo cerebral imaging with sufficient spatial integration of fluorescence intensity.[30] As expected, all of the derivatives showed emission wavelengths beyond 600 nm in dichloromethane, which were much longer than that of **PAD-1** (571 nm) (Table 1). **PAD-2**, **PAD-4**, and **PAD-6** with lengthened vinyl chains showed obvious emission redshift, compared to the emission spectra of **PAD-1**, **PAD-3**, and **PAD-5**, respectively. **PAD-2** to **PAD-5** exhibited good fluorescence quantum yields, which were considerably higher than that of ThT (0.01).[34] Besides, excellent fluorescence response was observed upon mixing with aggregated β-amyloid fibrils: **PAD-2**, **PAD-3**, and **PAD-4** showed brighter fluorescence (23, 15, and 17 fold increase in fluorescence intensity respectively) than that of **PAD-1** (7 fold), accompanied by significant blue shift in emission.[35] This may be caused by the restriction of conformational freedom upon binding to β-amyloid fibrils, decreasing the vibrational–rotational processes.[17] No significant change in fluorescence was observed during incubating **PAD-5** (or **PAD-6**) with β-amyloid fibrils, indicating that there is little or no interaction.

2.3. Binding ability for β-amyloid deposits

To investigate the specificity and affinity for β-amyloid deposits, fluorescence staining was performed using brain slices from a 12-month-old APP/PS1 transgenic mouse. APP/PS1 transgenic mice have been commonly used for in vitro and in vivo evaluations of β-amyloid specific probes because of marked cerebral β-amyloid deposition.[36] As shown in Figure 2, microscopic images of brain slices with **PAD-2**, **PAD-3**, and **PAD-4** staining showed extensive fluorescent labeling of β-amyloid deposits, while brain images with **PAD-5** and **PAD-6** staining displayed no specific labeling. The distribution of β-amyloid deposits was confirmed by staining of the adjacent brain slices with thioflavin S (ThS), which is a common dye for β-amyloid deposits.[37] Despite of its common use for histological demonstration of β-amyloid fibrils, ThS is not suitable for quantitative analysis: ThS is a complex mixture of methylated, sulfonated polymerized primulin preparation with uncharacterized structure; it exhibits brighter fluorescence without changes in the excitation or emission spectra upon binding to β-amyloid fibrils, resulting in high background fluorescence.[38] Saturation assay was then performed to quantify the binding affinity (Table 2). The affinity for aggregated β-amyloid fibrils varied: **PAD-2** and **PAD-4** showed higher affinity than that of **PAD-1**, with dissociation constant (K_d) values of 39.7 and 26.6 nM respectively; **PAD-3** displayed moderate affinity with K_d value of 94.0 nM, while **PAD-5** and **PAD-6** showed very poor affinity with K_d values over 10,000. These quantitative data were in accordance with fluorescent staining study.

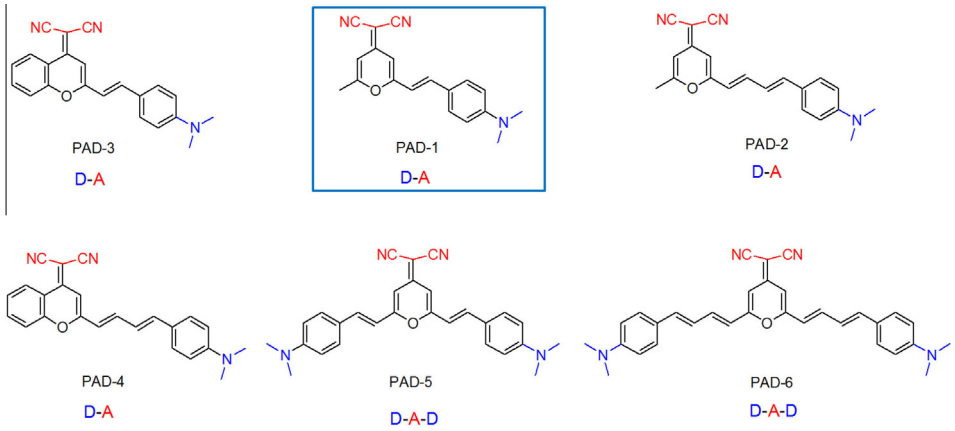

Figure 1. Chemical structure of styrylpyran derivatives.

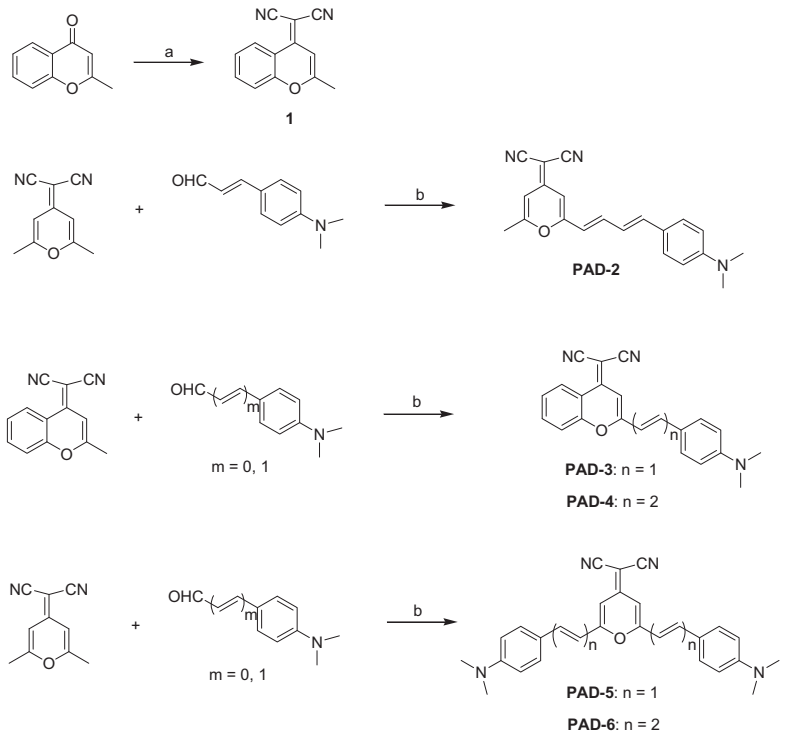

Scheme 1. Reagents and conditions: (a) malononitrile, acetic anhydride, 140 °C; (b) piperidine, acetonitrile, reflux.

Table 1
Fluorescence profile of styrylpyran derivatives

Compd	Mw	Log*P*[a]	λ_{abs}[b] (nm)	ε[b] (M^{-1} cm^{-1})	λ_{ex}[b] (nm)	λ_{em}[b] (nm)	Φ_F[b]	Fluorescence increase fold[c]	Emission blueshift[c]
PAD-1	303	2.06	467	43,180	478	571	0.48	7	46
PAD-2	329	2.58	487	39,860	492	636	0.29	23	50
PAD-3	339	3.79	515	67,244	519	646	0.19	15	50
PAD-4	365	4.31	523	68,516	524	657	0.10	17	40
PAD-5	434	4.26	485	75,530	492	613	0.64	/	/
PAD-6	486	5.29	502	44,440	507	661	0.02	/	/
ThT[d]	319	/	432	/	/	504	0.01	1000	/

[a] Log*P* values were calculated using ChemDraw Ultra 8.0.
[b] Maximum absorbance wavelength (λ_{abs}), molar absorption coefficient (ε), maximum excitation wavelength (λ_{ex}), maximum emission wavelength (λ_{em}), and fluorescence quantum yield (Φ_F) measured in CH_2Cl_2.
[c] Data measured in PBS with 2.75 μM $A\beta_{1-42}$ aggregates.
[d] Data from Ref. 34.

2.4. Molecular docking analysis

To get insight into possible interaction mechanism for β-amyloid binding, molecular docking analysis was carried out using GOLD software on 2-fold $A\beta_{1-40}$ fibril structure (PDB ID: 2LMO).[39–41] $A\beta_{1-42}$ shares the same residues as $A\beta_{1-40}$ with only one difference of two extra residues at the C-terminus. GoldScore was used as the scoring function for binding affinity prediction (Table 2). Since GoldScore yielded excellent correlation with the experimental binding affinity data, the interaction of these derivatives with active site residues was studied using the top-ranked binding pose of each compound from GoldScore (Fig. 3). For **PAD-1** or **PAD-2**, both donor and acceptor parts of the molecule are located within the hydrophobic binding pocket of the aggregated $A\beta_{1-40}$ fibril: the benzene ring forms hydrophobic interaction with PHE19, and *N*-methyl group forms hydrophobic interactions with PHE19 and ALA21; the cyano group has a hydrogen-bonding interaction with ILE31. For **PAD-3** or **PAD-4**, the benzene ring of benzopyran forms hydrophobic interaction with PHE19, and the cyano group forms a hydrogen-bonding interaction with ILE31. For **PAD-5** or **PAD-6**, the molecule is partially inserted into the binding pocket. The binding modes of these compounds revealed that hydrophobic interactions and hydrogen bonds are important contributions for their binding affinity, and the hydrophobic microenvironment with a lower dielectric constant may lead to an increase in fluorescence intensity and blue shift in emission. Besides, small and nearly planar molecules (**PAD-1** to **PAD-4**) insert into the binding site easily, while large stereo–hindrance hampers the interaction with β-amyloid fibril (**PAD-5** and **PAD-6**).

2.5. Brain uptake

Permeability of blood–brain barrier (BBB) is crucial for in vivo imaging of cerebral β-amyloid deposits. To investigate BBB penetration, brain uptake of high-affinity compounds (**PAD-2**, **-3**, and **-4**) were evaluated in normal mice. The compounds have small molecules (<400 Da) and suitable lipophilicity (calculated Log*P* values between 2 and 5), indicating that they could potentially cross BBB by passive diffusion (Table 1).[5] As expected, all compounds penetrated BBB rapidly and washed out from the brain

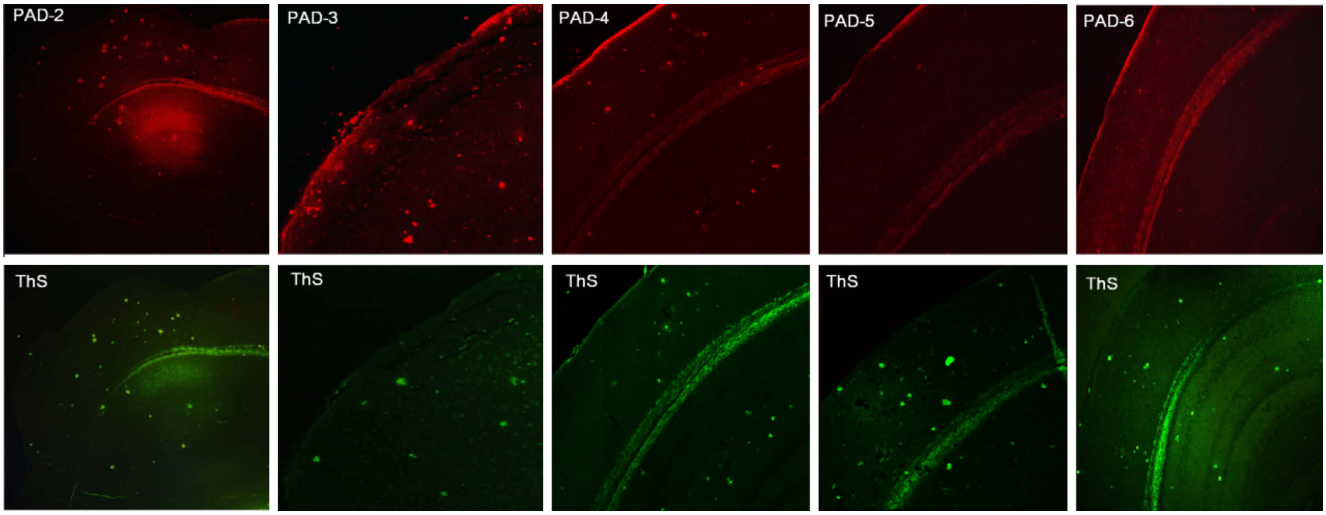

Figure 2. Neuropathological staining of brain slices from an APP/PS1 transgenic mouse (male, 12-month-old). (a) Staining with styrylpyran derivatives (upper). (b) Adjacent slices were stained with thioflavin S to confirm the presence of β-amyloid plaques (below).

Table 2
Dissociation constant (K_d) and GoldScore of styrylpyran derivatives

Compd	K_d[a] (nM)	GoldScore
PAD-1	58.9 ± 10.2	66.5
PAD-2	39.7 ± 9.1	67.8
PAD-3	94.0 ± 20.6	61.8
PAD-4	26.6 ± 6.3	70.6
PAD-5	>10,000	45.9
PAD-6	>10,000	33.3

[a] Values are the means ± standard errors of the mean of 6 independent determinations.

with time (Fig. 4). The molecular weight and *c*Log*P* of **PAD-2** were a little higher than those of **PAD-1**, and lower than those of **PAD-3** and **PAD-4**. Notably, the clearance of **PAD-2** from the brain was similar to that of **PAD-1**, and much faster than that of **PAD-3** and **PAD-4**, suggesting that **PAD-2** could contribute minimally to the background signal. Thus, **PAD-2**, with rapid BBB penetration and fast washout from the brain, was selected for further cerebral imaging in transgenic mice.

2.6. In vivo imaging

Finally, imaging in APP/PS1 transgenic mice and wild type control mice was conducted to assess the potential of **PAD-2** for noninvasive detection of cerebral β-amyloid deposits. As shown in Figure 5, fluorescence signals were captured in the brain area, indicating that **PAD-2** could penetrate BBB effectively. Fluorescence intensity of brains in APP/PS1 transgenic mice decreased more slowly than in wild type controls, which may be contributed to the specific labeling of cerebral β-amyloid deposits. Ex vivo histological observation was performed to further confirm the binding of **PAD-2** to cerebral β-amyloid deposits in vivo. Microscopic images of APP/PS1 brain slices showed distinct labeling of β-amyloid plaques, while no labeling was observed in wild type controls owing to the absence of β-amyloid plaques (Fig. 6). **PAD-2** has slightly lower quantum yield than that of **PAD-1**, but makes up for this deficiency by displaying longer emission wavelength, higher affinity to β-amyloid deposits, and intensively brighter fluorescence upon β-amyloid binding. In vivo and ex vivo studies demonstrated that **PAD-2** could specifically label cerebral β-amyloid deposits in vivo. Also, the improved properties of **PAD-2** overcame the difficulties of charged Thioflavin dyes (ThT/ThS), such as limited BBB permeability and high autofluorescence from biological matter during in vivo imaging, making **PAD-2** a potentially useful fluorescence probe for noninvasive detection of cerebral β-amyloid deposits.

3. Conclusions

In conclusion, a series of styrylpyran fluorophores were designed and evaluated for targeted detection of cerebral β-amyloid deposits. In vitro evaluation showed that styrylpyran motif has specificity towards β-amyloid deposits and fluorescence changes upon β-amyloid binding, which could provide a new scaffold for the development of optical probes targeting cerebral β-amyloid deposits. Among these derivatives, **PAD-2** displayed improved characteristics compared to **PAD-1**. **PAD-2** could discriminate APP/PS1 transgenic mice from wild type controls, with specific labeling of cerebral β-amyloid deposits in vivo, suggesting its potential application for targeted detection of β-amyloid deposits both in vitro and in vivo.

4. Experimental section

4.1. Material and methods

All chemicals and solvents were commercial products and were used without further purification. ^{1}H NMR spectra were recorded at 400 MHz on a varian INOVA 400 M NMR spectrometer in $CDCl_3$ solutions with tetramethylsilane (TMS) as an internal standard at room temperature. Chemical shifts are reported as δ values relative to the internal TMS. Coupling constants are reported in Hertz. Multiplicity is defined by s (singlet), d (doublet), t (triplet), or m (multiplet). Mass spectra were acquired using an Agilent 6410B Triple Quadrupole LC/MS system (ESI). HPLC was performed with a Shimadzu system (a LC-10AT pump with a SPD-10A UV detector, λ = 254 nm) with a Cosmosil C18 column (Nakalai Tesque, 5C_{18}-AR-II, 4.6 mm × 150 mm) using a mobile phase (water/acetonitrile: 3/7) delivered at a flow rate of 1.0 mL/min. UV/vis and fluorescence spectra were measured by UV-3600 and RF5301PC spectrophotometers (Shimadzu, Japan), respectively. Fluorescent observation was performed using Aviovert 40 CFL microscope (Zeiss, Germany). All key compounds were proven to show ⩾99% purity by analytical HPLC. Animal studies were carried out in full

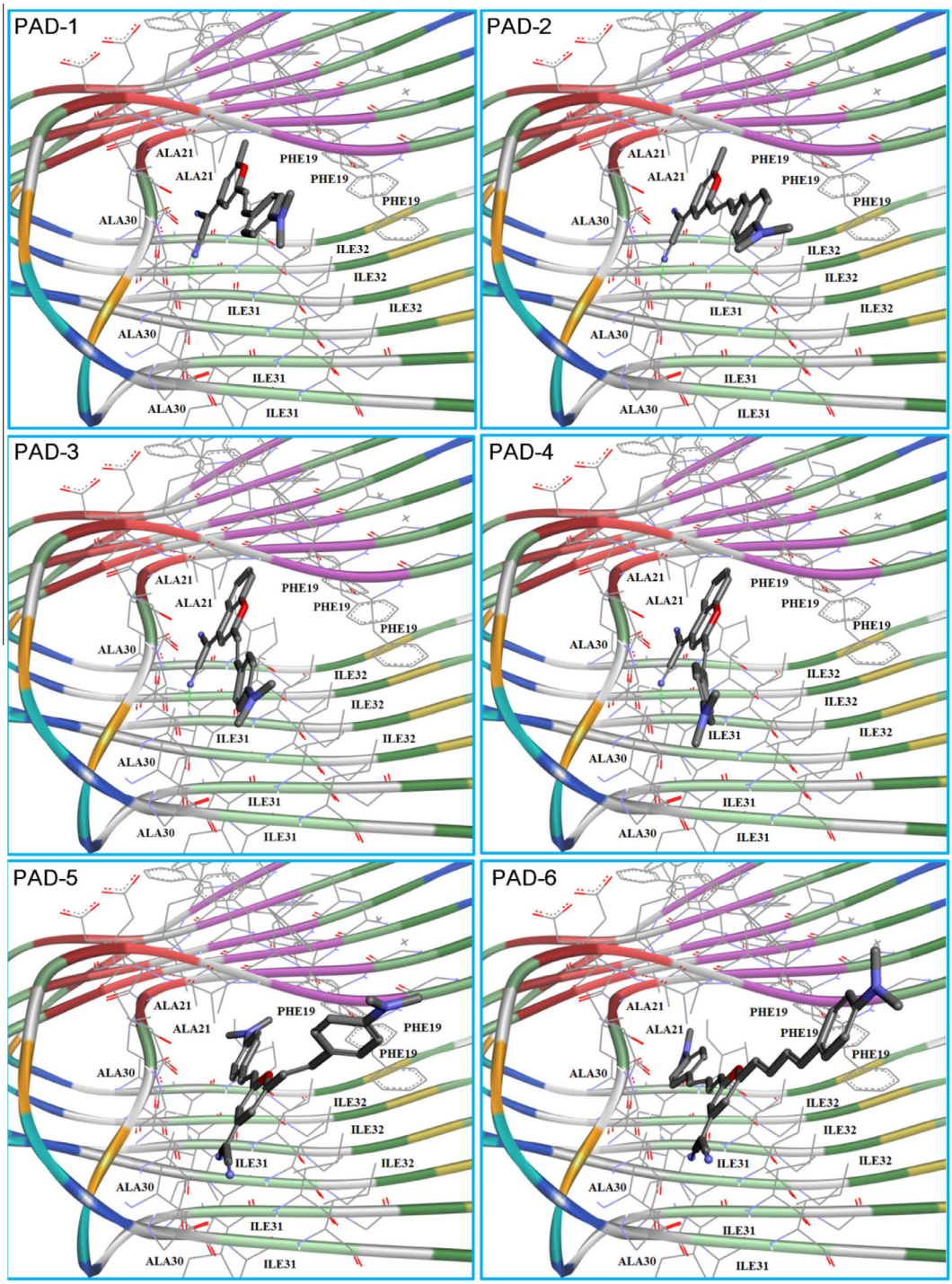

Figure 3. Computational binding models of compounds (**PAD-1** to **PAD-6**) with 2-fold Aβ fibrils. Side chains of PHE19, ALA21, ALA30, ILE31, and ILE32 are shown in stick form.

compliance with the regulations of Animal Care and Use Committee of Sichuan University.

4.2. Chemistry

4.2.1. General procedure A

To a solution of (2,6-dimethyl-4*H*-pyran-4-ylidene)malononitrile (1 mmol) and substituted aromatic aldehydes (1–2 mmol) in acetonitrile (10 mL) was added piperidine (200 μL). The reaction mixture was stirred under reflux for 12 h. The precipitate was collected by filtration and recrystallized from ethanol or purified by silica gel chromatography to afford the final products.

4.2.2. General procedure B

To a solution of compound **1** (1 mmol) and substituted aromatic aldehydes (1 mmol) in acetonitrile (10 mL) was added piperidine (200 μL). The reaction mixture was stirred under reflux for 10 h. The precipitate was collected by filtration and recrystallized from ethanol or purified by silica gel chromatography to afford the final products.

Please cite this article in press as: Zhu, B.-y.; et al. *Bioorg. Med. Chem.* (2016), http://dx.doi.org/10.1016/j.bmc.2016.01.004

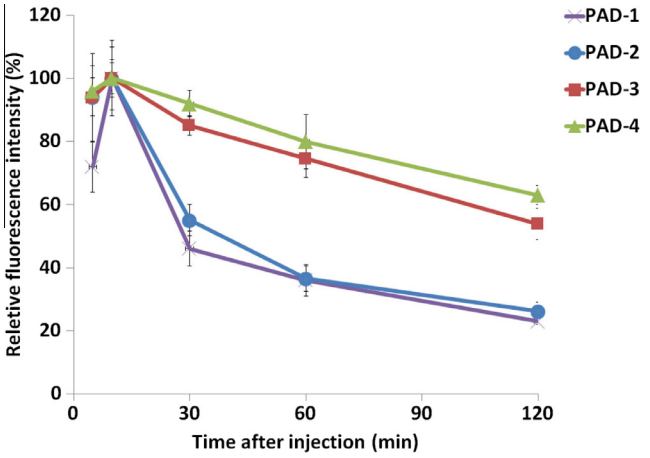

Figure 4. Comparison of brain uptake of **PAD-1**, **-2**, **-3**, and **-4** in normal mice ($n = 5$ at each time point).

4.2.3. 2-(2-Methyl-4*H*-chromen-4-ylidene)malononitrile (1)

Malononitrile (1.44 g, 21.8 mmol) was added to a stirring solution of 2-methylchromone (3.10 g, 19.4 mmol) in acetic anhydride (4 mL). The reaction mixture was stirred at 140 °C for 20 h. The reaction mixture was cooled to room temperature and filtered. The crude solid was recrystallized from ethanol to give 1.58 g of **1** (39.3%). ^{1}H NMR (400 MHz, $CDCl_3$): δ 2.44 (s, 3H), 6.73 (s, 1H), 7.25–7.45 (m, 2H), 7.62–7.70 (m, 1H), 8.92 (d, 1H, $J = 8.4$ Hz).

4.2.4. 2-(2-((1*E*,3*E*)-4-(4-(Dimethylamino)phenyl)buta-1,3-dienyl)-6-methyl-4*H*-pyran-4-ylidene)malononitrile (PAD-2)

PAD-2 was prepared following general procedure A (yield: 20.5%). ^{1}H NMR (400 MHz, $CDCl_3$): δ 2.33 (s, 3H), 3.04 (s, 6H), 6.14 (d, 1H, $J = 14.8$ Hz), 6.49 (s, 1H), 6.55 (s, 1H), 6.75 (d, 2H, $J = 8.4$ Hz), 6.78 (d, 2H, $J = 11.2$ Hz), 6.86 (d, 1H, $J = 15.6$ Hz), 7.39 (d, 2H, $J = 8.4$ Hz). MS: m/z 330 (M^++H).

4.2.5. (*E*)-2-(2-(4-(Dimethylamino)styryl)-4*H*-chromen-4-ylidene)malononitrile (PAD-3)

PAD-3 was prepared following general procedure B (yield: 30.7%). ^{1}H NMR (400 MHz, $CDCl_3$, ppm): δ 3.08 (s, 6H), 6.58 (d, 1H, $J = 16.0$ Hz), 6.75 (d, 2H, $J = 8.4$ Hz) 6.78 (s, 1H), 7.40–7.42 (m, 1H), 7.49 (d, 2H, $J = 8.4$ Hz), 7.54 (d, 1H, $J = 6.0$ Hz), 7.60 (s, 1H), 7.69–7.73 (m, 1H), 8.90 (d, 1H, $J = 8.4$ Hz). MS: m/z 340 (M^++H).

4.2.6. 2-(2-((1*E*,3*E*)-4-(4-(Dimethylamino)phenyl)buta-1,3-dienyl)-4*H*-chromen-4-ylidene)malononitrile (PAD-4)

PAD-4 was prepared following general procedure B (yield: 26.6%). ^{1}H NMR (400 MHz, $CDCl_3$, ppm): δ 3.06 (s, 6H), 6.58 (d, 1H, $J = 10.8$ Hz), 6.74 (d, 2H, $J = 4.8$ Hz) 6.79 (s, 1H), 7.41–7.43 (m, 2H), 7.50 (d, 2H, $J = 6.0$ Hz), 7.53 (d, 1H, $J = 5.6$ Hz), 7.58 (d, 1H, $J = 10.8$ Hz), 7.69–7.72 (m, 2H), 8.91 (d, 1H, $J = 6.0$ Hz). MS: m/z 366 (M^++H).

4.2.7. 2-(2,6-Bis((*E*)-4-(dimethylamino)styryl)-4*H*-pyran-4-ylidene)malononitrile(PAD-5)

PAD-5 was prepared following general procedure A (yield: 20.5%). ^{1}H NMR (400 MHz, $CDCl_3$, ppm): δ 3.06 (s, 12H), 6.56 (d, 1H, $J = 8.4$ Hz), 6.77 (d, 4H, $J = 6.8$ Hz), 7.44 (s, 2H), 7.48 (d, 2H, $J = 8.4$ Hz). MS: m/z 435 (M^++H).

4.2.8. 2-(2,6-Bis((1*E*,3*E*)-4-(4-(dimethylamino)phenyl)buta-1,3-dienyl)-4*H*-pyran-4-ylidene)malononitrile (PAD-6)

PAD-6 was prepared following general procedure A (yield: 17.2%). ^{1}H NMR (400 MHz, $CDCl_3$, ppm): δ 3.09 (s, 12H), 6.24 (d, 2H, $J = 15.6$ Hz), 6.54 (s, 2H), 6.81–6.88 (m, 2H), 6.94 (d, 4H, $J = 15.2$ Hz), 7.30–7.33 (m, 2H), 7.48 (d, 4H, $J = 8.0$ Hz). MS: m/z 487 (M^++H).

4.3. Biological evaluation

4.3.1. Preparation of aggregated β-amyloid fibrils

$A\beta_{1-42}$ peptide (Amresco, USA) was gently dissolved in PBS solution (pH 7.4) containing 1 mM EDTA. The solution (0.25 mg/mL) was incubated at 37 °C for 42 h with gentle and constant shaking.

4.3.2. Spectroscopic characterization

Maximum absorbance wavelength (λ_{abs}), molar absorption coefficient (ε), maximum excitation wavelength (λ_{ex}), maximum emission wavelength (λ_{em}), and fluorescence quantum yield (Φ_F) were measured in dichloromethane.[19] Rhodamine B (Sigma, USA) was taken as a reference for determining fluorescence quantum yields. Each compound (1.0 μM, final concentration) was dissolved in PBS solution alone or a prepared solution of $A\beta_{1-42}$ aggregates (2.75 μM, final concentration) in PBS to test interactions of each

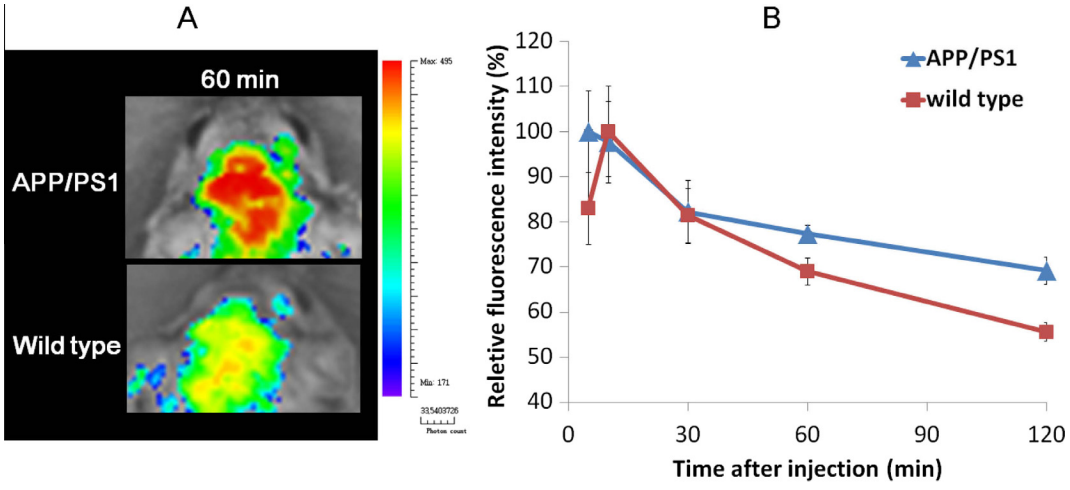

Figure 5. In vivo imaging of APP/PS1 transgenic mice and wild type controls after intravenous injection of **PAD-2**. (A) Images at 60 min postinjection; (B) quantitative analysis of fluorescence intensity at different timepoint.

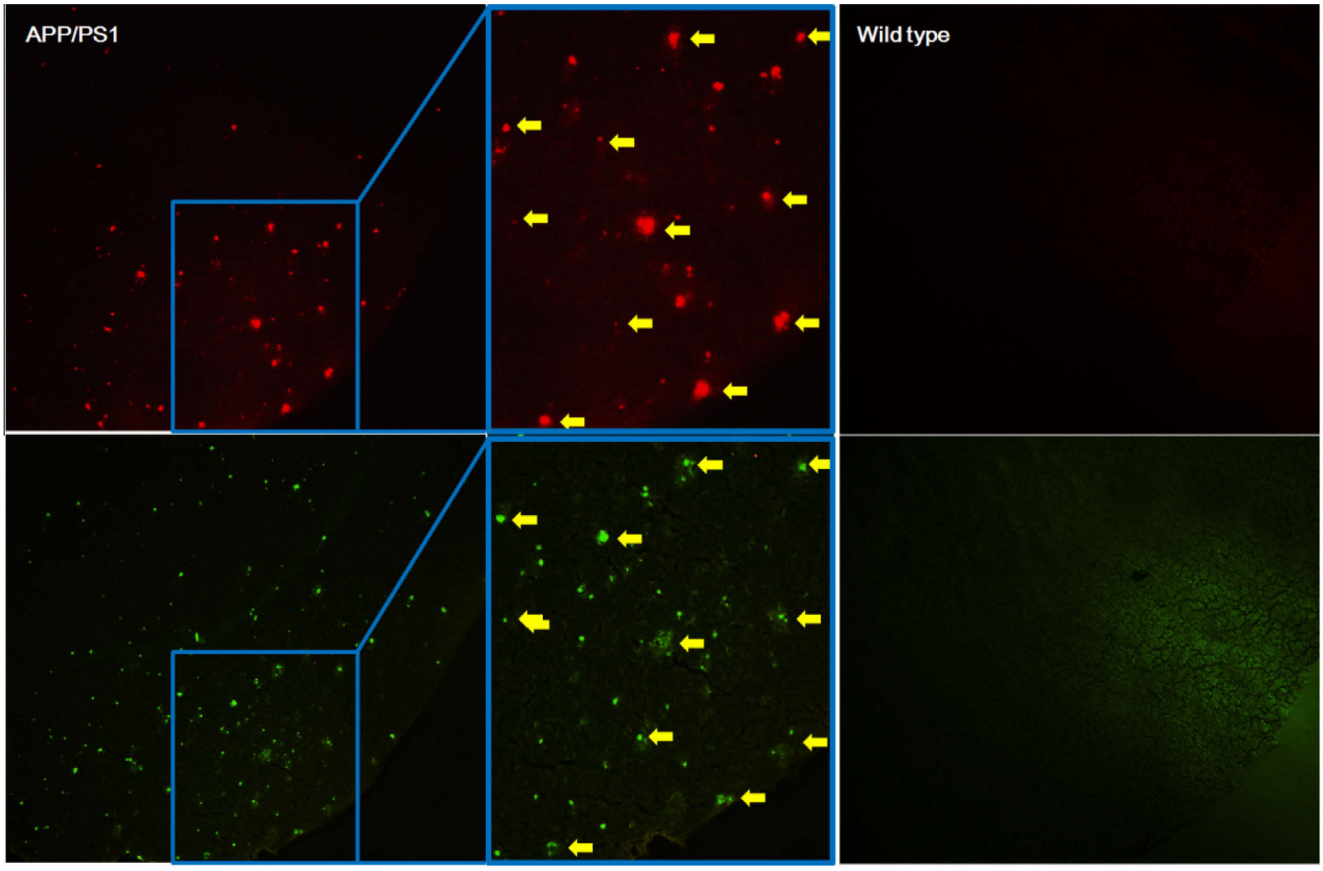

Figure 6. Ex vivo histological observation of brain slices from APP/PS1 transgenic mice and wild type controls after intravenous injection of **PAD-2** (upper). The adjacent brain slices were stained with thioflavin S to localize β-amyloid plaques (below).

compound with β-amyloid aggregates (fluorescence increase and blueshift).

4.3.3. In vitro fluorescence staining of APP/PS1 brain tissue

Brain sections from an aged APP/PS1 transgenic mouse (male, 12 months, 15 μm) were incubated with each compound (1.0 μM in 30% ethanol) for 5–10 min at room temperature. The localization of β-amyloid plaques was confirmed by staining the adjacent brain sections with thioflavin S (0.125%). The sections were then washed with 40% ethanol (two 2-min washes), rinsed with water for 30 s. After drying at room temperature, fluorescent observation was then performed with FITC and GFP filter sets.

4.3.4. In vitro binding assays using aggregated β-amyloid fibrils

Binding affinity of each compound was assessed by saturation assays with $A\beta_{1-42}$ aggregates in PBS solution. A mixed PBS solution containing each compound (1 nM–10 μM) and $A\beta_{1-42}$ aggregates (1.5 μM) was incubated at room temperature for 1 h and transferred to a black 96-well plate to measure fluorescent intensity by a multifunction microplate reader (Thermo Scientific Varioskan Flash, USA). Dissociation constant (K_d) was calculated using GraphPad Prism 5.0 (GraphPad Software, Inc., USA).

4.3.5. Biodistribution experiments with normal mice

Kunming mice (8 weeks, male) were intravenously injected with 50 μL of each compound (2.0 mg/kg, 20% DMSO, 80% propylene glycol). The mice were sacrificed at 5, 30, 60, 120 min postinjection and whole brains were taken out (n = 5 at each time point). Fluorescence signals were then recorded and analyzed using a QuickView 3000 imaging system with QuickView 3000 software (BioReal, Austria). Intensity of brain fluorescence at each timepoint [$F(t)$] was calculated from the photon counts and was normalized by the subtraction of preinjected background signals [$F(pre)$]. Relative fluorescence intensity (%) at each timepoint was calculated by the following equation:

$$\text{Relative fluorescence intensity} = [F(t) - F(pre)]/[F(t') - F(pre)] \times 100\% \quad \text{(I)}$$

$F(t')$ represents the highest intensity for each compound.

4.3.6. In vivo analysis of PAD-2 on APP/PS1 transgenic mice

The QuickView 3000 imaging system was used to perform in vivo imaging. Images were obtained with a customized 534-nm excitation filter and 716-nm emission filter. QuickView 3000 software was used for data analysis. 16-Month-old APP/PS1 transgenic mice and corresponding wild-type control mice were shaved before background imaging. **PAD-2** (2.0 mg/kg, 20% DMSO, 80% propylene glycol) was injected into the mice through tail vein. Real-time images were recorded and Regions of Interest (ROIs) were drawn covering the whole brain. The data were analyzed using the Eq. I.

4.3.7. Ex vivo examination of β-amyloid labeling

After in vivo imaging at 120 min postinjection, the mice were immediately sacrificed by decapitation. For microscopic observation, the brains were sliced (15-μm-thick) using a CM1950 cryostat (Leica, Germany). After drying, the brain slices were observed using a microscope equipped with a FITC filter set. The adjacent slices were stained with thioflavin S to localize β-amyloid plaques, and were observed using the same microscope with a GFP filter set.

Please cite this article in press as: Zhu, B.-y.; et al. *Bioorg. Med. Chem.* (2016), http://dx.doi.org/10.1016/j.bmc.2016.01.004

4.4. Computational study

All of the docking process was carried out using GOLD 5.0 program, which is based on genetic algorithm.[24] A segment of $A\beta_{1-40}$ fibril was extracted from RCSB Protein Data Bank (PDB ID: 2LMO) and used as the reference receptor. Prior to molecular docking, the preparation of $A\beta_{1-40}$ fibril structure, including the addition of hydrogen atoms, deletion of water molecules, and assigning of Charmm force field, was performed using Discovery Studio 3.1 software package. A sphere including residues ALA30, ILE31, ILE32, PHE19, PHE20, and ALA21 were defined as the binding site. GoldScore scoring function was used to identify docking poses as well as to rank these poses. 30 docking runs were set for each compound. The best docking pose was preserved and corresponding scoring values was extracted.

Acknowledgments

The study was supported by the National Natural Science Foundation of China (81402891), Ph.D. Programs Foundation of Ministry of Education of China (20130181120114), and China Postdoctoral Science Foundation Grant (2014M560723).

Supplementary data

Supplementary data associated with this article can be found, in the online version, at http://dx.doi.org/10.1016/j.bmc.2016.01.004.

References and notes

1. Glenner, G. G.; Wong, C. W. *Biochem. Biophys. Res. Commun.* **1984**, *122*, 1131.
2. Chiti, F.; Dobson, C. M. *Annu. Rev. Biochem.* **2006**, *75*, 333.
3. Hardy, J.; Selkoe, D. J. *Science* **2002**, *297*, 353.
4. Selkoe, D. J. *Nat. Biotechnol.* **2000**, *18*, 823.
5. Mathis, C. A.; Wang, Y.; Klunk, W. E. *Curr. Pharm. Des.* **2004**, *10*, 1469.
6. Ono, M.; Wilson, A.; Nobrega, J.; Westaway, D.; Verhoeff, P.; Zhuang, Z. P.; Kung, M. P.; Kung, H. F. *Nucl. Med. Biol.* **2003**, *30*, 565.
7. Mathis, C. A.; Wang, Y.; Holt, D. P.; Huang, G. F.; Debnath, M. L.; Klunk, W. E. *J. Med. Chem.* **2003**, *46*, 2740.
8. Klunk, W. E.; Engler, H.; Nordberg, A.; Wang, Y.; Blomqvist, G.; Holt, D. P.; Bergstrom, M.; Savitcheva, I.; Huang, G. F.; Estrada, S.; Ausen, B.; Debnath, M. L.; Barletta, J.; Price, J. C.; Sandell, J.; Lopresti, B. J.; Wall, A.; Koivisto, P.; Antoni, G.; Mathis, C. A.; Langstrom, B. *Ann. Neurol.* **2004**, *55*, 306.
9. Koole, M.; Lewis, D. M.; Buckley, C.; Nelissen, N.; Vandenbulcke, M.; Brooks, D. J.; Vandenberghe, R.; Van Laere, K. *J. Nucl. Med.* **2009**, *50*, 818.
10. Villemagne, V. L.; Ong, K.; Mulligan, R. S.; Holl, G.; Pejoska, S.; Jones, G.; O'Keefe, G.; Ackerman, U.; Tochon-Danguy, H.; Chan, J. G.; Reininger, C. B.; Fels, L.; Putz, B.; Rohde, B.; Masters, C. L.; Rowe, C. C. *J. Nucl. Med.* **2011**, *52*, 1210.
11. Choi, S. R.; Golding, G.; Zhuang, Z. P.; Zhang, W.; Lim, N.; Hefti, F.; Benedum, T. E.; Kilbourn, M. R.; Skovronsky, D.; Kung, H. F. *J. Nucl. Med.* **2009**, *50*, 1887.
12. Clark, C. M.; Schneider, J. A.; Bedell, B. J.; Beach, T. G.; Bilker, W. B.; Mintun, M. A.; Pontecorvo, M. J.; Hefti, F.; Carpenter, A. P.; Flitter, M. L.; Krautkramer, M. J.; Kung, H. F.; Coleman, R. E.; Doraiswamy, P. M.; Fleisher, A. S.; Sabbagh, M. N.; Sadowsky, C. H.; Reiman, E. P.; Zehntner, S. P.; Skovronsky, D. M. *JAMA* **2011**, *305*, 275.
13. Ono, M.; Cheng, Y.; Kimura, H.; Cui, M.; Kagawa, S.; Nishii, R.; Saji, H. *J. Med. Chem.* **2011**, *54*, 2971.
14. *J. Nucl. Med.* **2012**, *53*, 15N.
15. Sabri, O.; Seibyl, J.; Rowe, C.; Barthel, H. *Clin. Transl. Imaging* **2015**, *3*, 13.
16. Thal, D. R.; Beach, T. G.; Zanette, M.; Heurling, K.; Chakrabarty, A.; Ismail, A.; Smith, A. P.; Buckley, C. *Alzheimers Dement.* **2015**, *8*, 975.
17. Nesterov, E. E.; Skoch, J.; Hyman, B. T.; Klunk, W. E.; Bacskai, B. J.; Swager, T. M. *Angew. Chem., Int. Ed.* **2005**, *44*, 5452.
18. Weissleder, R.; Pittet, M. J. *Nature* **2008**, *452*, 580.
19. Hintersteiner, M.; Enz, A.; Frey, P.; Jaton, A. L.; Kinzy, W.; Kneuer, R.; Neumann, U.; Rudin, M.; Staufenbiel, M.; Stoeckli, M.; Wiederhold, K. H.; Gremlich, H. U. *Nat. Biotechnol.* **2005**, *23*, 577.
20. Okamura, N.; Mori, M.; Furumoto, S.; Yoshikawa, T.; Harada, R.; Ito, S.; Fujikawa, Y.; Arai, H.; Yanai, K.; Kudo, Y. *J. Alzheimers Dis.* **2011**, *23*, 37.
21. Cui, M.; Ono, M.; Watanabe, H.; Kimura, H.; Liu, B.; Saji, H. *J. Am. Chem. Soc.* **2014**, *136*, 3388.
22. Ran, C.; Xu, X.; Raymond, S. B.; Ferrara, B. J.; Neal, K.; Bacskai, B. J.; Medarova, Z.; Moore, A. *J. Am. Chem. Soc.* **2009**, *131*, 15257.
23. Zhang, X.; Tian, Y.; Li, Z.; Tian, X.; Sun, H.; Liu, H.; Moore, A.; Ran, C. *J. Am. Chem. Soc.* **2013**, *135*, 16397.
24. Chang, W. M.; Dakanali, M.; Capule, C. C.; Sigurdson, C. J.; Yang, J.; Theodorakis, E. A. *ACS Chem. Neurosci.* **2011**, *2*, 249.
25. Cao, K.; Farahi, M.; Dakanali, M.; Chang, W. M.; Sigurdson, C. J.; Theodorakis, E. A.; Yang, J. *J. Am. Chem. Soc.* **2012**, *134*, 17338.
26. Ono, M.; Ishikawa, M.; Kimura, H.; Hayashi, S.; Matsumura, K.; Watanabe, H.; Shimizu, Y.; Cheng, Y.; Cui, M.; Kawashima, H.; Saji, H. *Bioorg. Med. Chem. Lett.* **2010**, *20*, 3885.
27. Ono, M.; Watanabe, H.; Kimura, H.; Saji, H. *ACS Chem. Neurosci.* **2012**, *3*, 319.
28. Watanabe, H.; Ono, M.; Matsumura, K.; Yoshimura, M.; Kimura, H.; Saji, H. *Mol. Imaging* **2013**, *12*, 338.
29. Zhou, K.; Fu, H.; Feng, L.; Cui, M.; Dai, J.; Liu, B. *Chem. Commun.* **2015**, 11665.
30. Fu, H.; Cui, M.; Zhao, L.; Tu, P.; Zhou, K.; Dai, J.; Liu, B. *J. Med. Chem.* **2015**, *58*, 6972.
31. Watanabe, H.; Ono, M.; Saji, H. *Chem. Commun.* **2015**, 17124.
32. Cheng, Y.; Zhu, B.; Deng, Y.; Zhang, Z. *Anal. Chem.* **2015**, *87*, 4781.
33. Tolmachev, A. I.; Kachkovskii, A. D.; Kudinova, M. A.; Kurdiukov, V. V.; Ksenzov, S.; Schrader, S. *Dyes Pigments* **2007**, *74*, 348.
34. Voropai, E. S.; Samtsov, M. P.; Kaplevskii, K. N.; Maskevich, A. A.; Stepuro, V. I.; Povarova, O. I.; Kuznetsova, I. M.; Turoverov, K. K.; Fink, A. L.; Uverskii, V. N. *J. Appl. Spectrosc.* **2003**, *70*, 868.
35. For more details, see the Supporting information.
36. Bilkei-Gorzo, A. *Pharmacol. Ther.* **2014**, *142*, 244.
37. Cheng, Y.; Ono, M.; Kimura, H.; Kagawa, S.; Nishii, R.; Kawashima, H.; Saji, H. *ACS Med. Chem. Lett.* **2010**, *1*, 321.
38. LeVine, H., III *Methods Enzymol.* **1999**, *309*, 274.
39. Xu, W.; Lucke, A. J.; Fairlie, D. P. *J. Mol. Graph. Model.* **2015**, *57*, 76.
40. Petkova, A. T.; Ishii, Y.; Balbach, J. J.; Antzutkin, O. N.; Leapman, R. D.; Delaglio, F.; Tycko, R. *Proc. Natl. Acad. Sci. U.S.A.* **2002**, *99*, 16742.
41. Cook, N. P.; Ozbil, M.; Katsampes, C.; Prabhakar, R.; Martí, A. A. *J. Am. Chem. Soc.* **2013**, *135*, 10810.